JOURNAL OF GEOPHYSICAL RESEARCH, VOL. 100, NO. B2, PAGES 2193–2209, FEBRUARY 10, 1995

Closure domains in magnetite

Özden Özdemir, Song Xu[1], and David J. Dunlop

Department of Physics, Erindale College, University of Toronto, Mississauga, Ontario, Canada

Abstract. We have observed clear arrays of closure domains at internal and external boundaries, such as crystal edges, cracks, and chemically altered regions, in a single crystal of magnetite, using the Bitter colloid technique with a {110} viewing plane. The common occurrence of closure domains in magnetite confirms the controlling role of magnetostatic energy in determining domain structures in strongly magnetic materials, first postulated by Landau and Lifschitz (1935). Closure domains also reconcile a long-standing discrepancy between the numbers of body domains observed in magnetite and the numbers predicted, which we show are much reduced when closure domains are taken into account. We verify experimentally that closure domains change their shape and internal structure depending on the crystallographic orientation of the boundary at which they form. When the boundary intersects the {110} viewing plane along a <111> easy axis, for example, at favorably oriented internal boundaries or cracks, the closure domains are asymmetric in shape and are bounded by 71° and 109° walls. However, when the boundary is a {111} crystal face, containing no <111> easy axis, the closure domains are symmetric in form and bounded by ≈90° walls. Closure domains of this latter type collect colloid densely along one of the two bounding walls, suggesting concentrations of magnetic poles, and the two walls are at angles of 70°-80° to each other, rather than the expected 90°. Several possible models are proposed to explain this behavior. Our study shows that internal domain structures in magnetite are relatively simple. Much more complicated structures appear on viewing surfaces that do not contain two sets of <111> easy axes. The lack of orientation of the viewing surface in most previous studies may account for the reported rarity of closure domains in magnetite. Closure domain arrays forming at the margin of a chemically altered area are the first reported evidence for a direct link between chemical alteration and domain structures that could result in remagnetization.

Introduction

Closure Domains

In pioneering theoretical work, before magnetic domain patterns had been observed directly, *Landau and Lifshitz* [1935] predicted that closure domains should form at the surface of ferromagnetic crystals (Figure 1a). They reasoned that closure domains would complete the flux circuit between oppositely magnetized body domains entirely within the crystal, eliminating surface and interior poles and reducing the magnetostatic energy to zero.

In iron, the spontaneous magnetization $\mathbf{M_S}$ lies along <100> magnetocrystalline easy axes and changes direction by 90° between body and closure domains (Figure 1a; the viewing plane is (100)). In order to make the net pole density $\sigma = \sum \mathbf{M_S}\cdot\hat{\mathbf{n}}$ zero on all internal boundaries ($\hat{\mathbf{n}}$ is an outward normal to the boundary), walls must bisect the angle between the $\mathbf{M_S}$ vectors in adjacent domains. As a result, 90° walls make angles of 135° with 180° walls and are perpendicular to each other (Figure 1a). No poles appear on external boundaries because $\mathbf{M_S}$ vectors in closure domains are in <100> easy directions, parallel to the {100} crystal surfaces. Both magnetostatic and magnetocrystalline energies have been eliminated.

In magnetite, $\mathbf{M_S}$ vectors are oriented in <111> easy directions and change direction by 70.5° or 109.5° between body and closure domains (Figure 1b; the viewing plane is (110), containing two easy axes, $[1\bar{1}1]$ and $[1\bar{1}\bar{1}]$). The 70.5° and 109.5° walls (usually called 71° and 109° walls for simplicity) are perpendicular, like the 90° walls in iron, but the angles they make with the 180° wall are 125° and 145°, respectively. These angles are necessary to ensure that $\sigma = \mathbf{M_{S1}}\cdot\hat{\mathbf{n}} + \mathbf{M_{Sc}}\cdot\hat{\mathbf{n}}_c = 0$ across the 71° wall and $\sigma' = \mathbf{M_{Sc}}\cdot\hat{\mathbf{n}}'_c + \mathbf{M_{S2}}\cdot\hat{\mathbf{n}}' = 0$ across the 109° wall. The 125° and 145° angles between walls can be measured directly using the Bitter technique, whereas the 71° and 109° angles between $\mathbf{M_S}$ vectors cannot.

In Figure 1b, $\mathbf{M_{Sc}}$ lies along a surface-parallel <111> easy axis, eliminating both magnetostatic and magnetocrystalline energies. In real magnetite crystals, the <111> axes usually make an angle with the crystal surfaces. For example, if the crystal is bounded by {111} octahedral faces (Figures 1c and 2), one <111> axis is perpendicular to the surface and the other three make angles of 19.5° with the surface. If $\mathbf{M_{Sc}}$ is along a <111> axis as in Figure 1c, it will intersect the surface, generating poles and magnetostatic energy. It is likely that a compromise is achieved, in which $\mathbf{M_{Sc}}$ near the surface rotates out of the <111> axis in order to be more nearly surface-parallel. We calculate this deflection in a later section.

[1]Now at NirvCentre, Toronto, Ontario, Canada.

Paper number 94JB02874.
0148-0227/95/94JB-02874$05.00

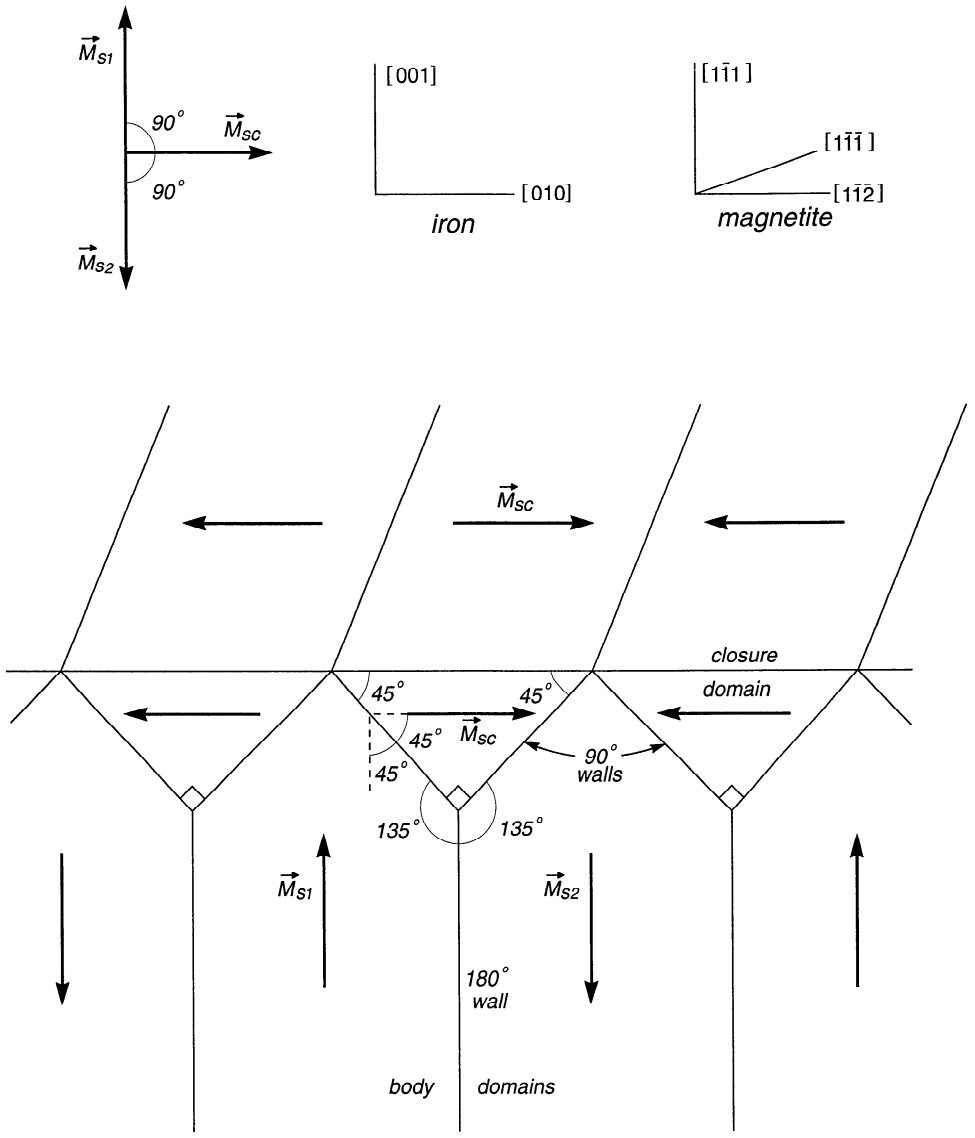

Figure 1a. Theoretical model of closure domains. The Landau and Lifschitz structure, appropriate to iron ($\mathbf{M_S}$ parallel to [001], $\mathbf{M_{SC}}$ parallel to [010]). It may also be relevant to magnetite ($\mathbf{M_S}$ parallel to [1$\bar{1}$1], $\mathbf{M_{SC}}$ parallel to [1$\bar{1}\bar{2}$]; see theory and discussion sections).

Observations of Closure Domains

In large single crystals with surfaces cut parallel to crystal planes containing easy directions of magnetization, it is possible to observe domain structures like those predicted by Landau and Lifschitz. In the present study, we examine the closure domain structures which form in a crystal of magnetite viewed on {110} and {111} planes. Because the {110} plane contains two sets of <111> easy axes, patterns observed in this plane are simple and probably closely resemble domain structures in the crystal interior. Patterns observed in {111} are complicated by extraneous structures arising from surface poles, but underlying structures can also be seen.

The earliest observations of closure domains in cubic crystals were made by H.J. Williams (shown by *Kittel* [1949]) on iron and by *Elscher and Andrä* [1955] on silicon-iron. On a {100} viewing plane, they observed sets of 180° body domains bounded at the crystal edge by 90° closure domains, exactly as in Figure 1a.

Closure domains have been observed only sporadically in magnetite. *Bogdanov and Vlasov* [1965] observed clear sets of 180° body domains on a {110} surface, but a blanket of colloid obscured the edges of the viewing surface. *Smith* [1980] (who used Lorentz electron microscopy rather than the Bitter colloid method) reported several examples of closure structures on ≈1-μm magnetite inclusions in garnet. The closure domains imaged poorly or not at all at the crystal edges, however.

Heider et al. [1988] and *Soffel et al.* [1990] reported a few examples of closure domains in ≈10-μm hydrothermally grown magnetite crystals. Heider et al.'s picture is particularly interesting because the closure domains are greatly reduced in size where two neighboring crystals touch. This observation confirms that closure structures exist to reduce magnetostatic energy and are unnecessary when the flux circuit can be

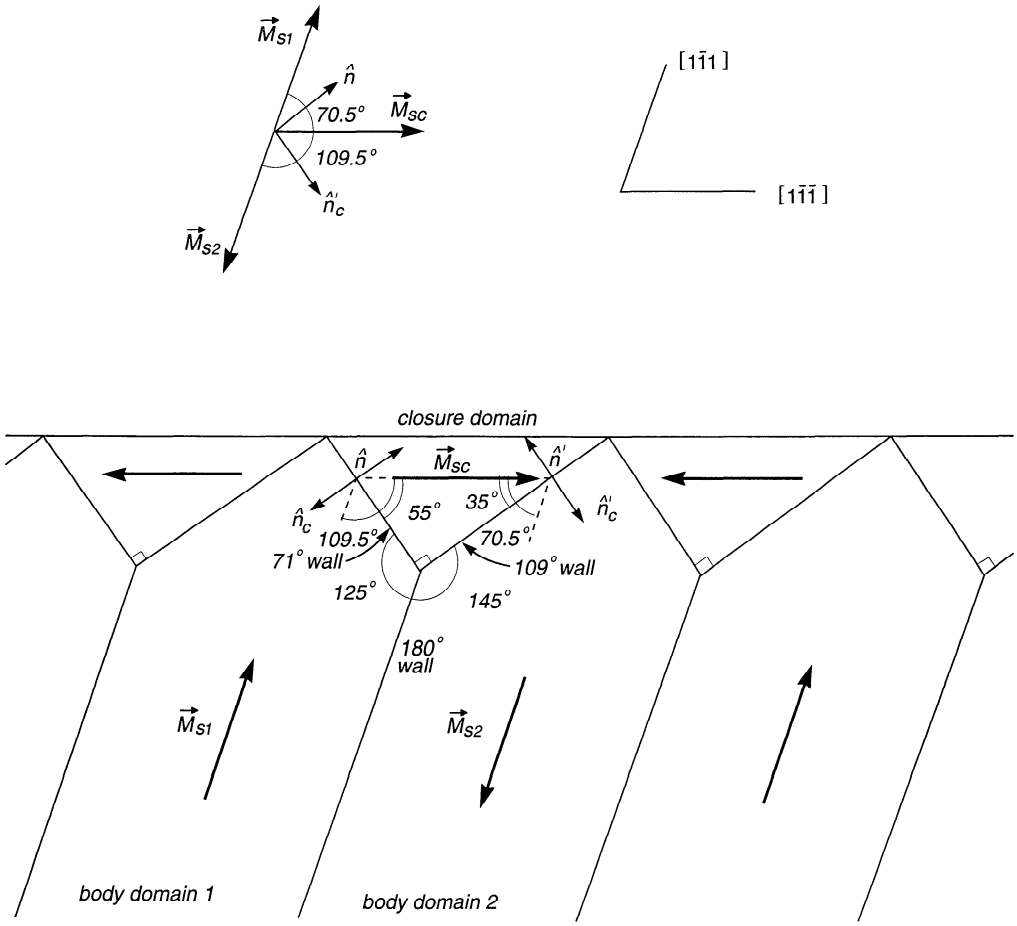

Figure 1b. Closure domains in magnetite, bounded by 71° and 109° walls. $\mathbf{M_{SC}}$ is parallel to [1$\bar{1}\bar{1}$].

completed in other ways, e.g., between body domains in adjacent crystals. We show an example in the present paper of domain interactions across a grain boundary.

Özdemir and Dunlop [1993] reported the first unequivocal examples of sets of surface closure domains in magnetite terminating body domains at the crystal edge. Why have closure structures so seldom been seen when theoretically they should be the principal means of reducing magnetostatic energy?

There are a number of technical problems. With new polishing methods, magnetostrictively generated maze patterns due to surface stresses can now be eliminated [*Hoffmann et al.*, 1987]. However, because magnetite has low magnetocrystalline anisotropy compared to iron, walls are broad and produce a weaker magnetic field gradient which attracts less colloid [*Soffel et al.*, 1990]. *Williams et al.* [1992] calculate that small-angle walls (71° and 109°, for example), whether they have Bloch or Néel (surface-parallel spin rotation) structure, attract less colloid than large-angle (180°) walls.

Sectioning a crystal to view domain structures modifies the structures one is trying to view. Only on a plane parallel within a degree or so to {110} does one have much hope of replicating interior structures. In any other orientation, one or more sets of <111> axes will cut the viewing surface, producing poles and extraneous structures. Few previous studies of magnetite, apart from Bogdanov and Vlasov's, have attempted to orient the viewing plane(s).

Even if the viewing plane is appropriate, one may be viewing the body domains or the closure domains broadside-on (left and top views, respectively, in Figure 1a), instead of edge-on. Viewed from above, the closure domains appear to be a set of 180° domains without edge terminations. The orientations of $\mathbf{M_S}$ vectors would disclose the true situation, but these are not evident from the Bitter patterns.

Edge topography may also play an important role. Even the most carefully polished section tends to have stepped or sloping edges. Throughout the edge zone, therefore, the viewing surface intersects <111> easy axes. The resulting poles generate fine structures which may accumulate colloid to such an extent that the edge zone is blanketed.

Much has been written about the discrepancy between the numbers of domains observed on titanomagnetite grains of a given size and the number predicted theoretically [e.g., *Worm et al.*, 1991]. However, if closure domains are taken into account, far fewer body domains are required, and the "missing domains paradox" disappears [*Xu et al.*, 1994]. Our observations, described in the rest of the paper, confirm that closure domains are a typical feature of the interior domain structure in magnetite. Although for technical reasons (namely, the need for precise crystallographic orientation in order to view domains

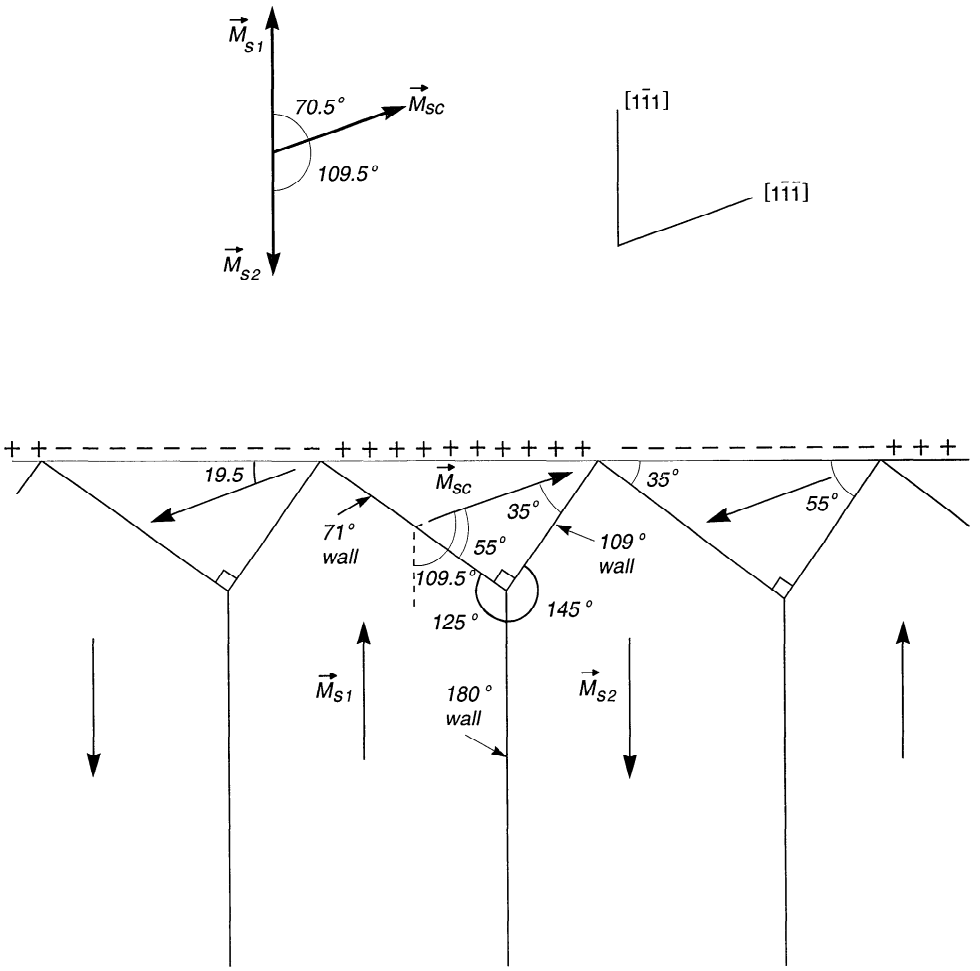

Figure 1c. $\mathbf{M_{sc}}$ vectors in <111> easy directions cut a {111} crystal surface, generating positive and negative poles.

without distortion) we have used large magnetite crystals, we believe that closure domains are typical of smaller grains as well. In the theory section, we will show how body and closure domains scale with grain size in the smaller multidomain and pseudo-single-domain grains that carry stable paleomagnetic remanences. There are enough observations on grains with fortuitously favorable orientations [*Smith*, 1980; *Heider et al.*, 1988; *Soffel et al.*, 1990] to demonstrate that closure domains do occur commonly in small grains, as our calculations predict. As a result, we doubt that there is a serious discrepancy between observations and predictions of the numbers of domains in magnetite.

Experimental Method and Sample Characterization

Domain observations were made on a 3-mm octahedral crystal of magnetite (Figure 2; ADEFGH represents the octahedron) in the laboratory ambient field of ≈ 60 μT. The crystal was oriented under a stereoscopic microscope by means of a laser beam reflected from a {111} face and then sectioned parallel to three different planes: {110}, represented by triangle ABC; {111}, represented by triangle ADE; and {100}, represented by square DEFG. The {110} plane is of particular interest because it contains four of the eight <111> directions of easy magnetization (Figure 2). Strain-free surfaces produced by final polishing with amorphous silica [*Hoffmann et al.*, 1987] greatly improved the clarity of the domain patterns observed.

Domain walls were observed by the Bitter technique in which colloidal ultrafine magnetite particles dispersed in a liquid carrier (Ferrofluid) decorate the intersections of domain walls with the viewing surface. A drop of oil-based Ferrofluid was placed on the polished surface and spread into a thin layer using a cover glass. The domain structures were then viewed and photographed using bright-field microscopy on a Nikon-Optiphot microscope. We used high-resolution oil immersion lenses with relatively short working distances.

Before the crystal was oriented and cut, room-temperature saturation hysteresis parameters were measured with a vibrating-sample magnetometer (Figure 3). The observed saturation magnetization of 86 A m^2/kg is lower than the expected 92 A m^2/kg for pure Fe_3O_4. The low M_s value is due to nonmagnetic impurities such as chlorite or biotite, which are common inclusions in natural magnetite crystals [*Özdemir and York*, 1992]. The saturation remanence ratio $M_{rs}/M_s = 0.003$ and the coercivity ratio $H_{cr}/H_c = 22.6$ indicate true multidomain behavior.

Figure 4 shows the behavior of a small chip of the crystal when it was given a saturation isothermal remanence (SIRM) at

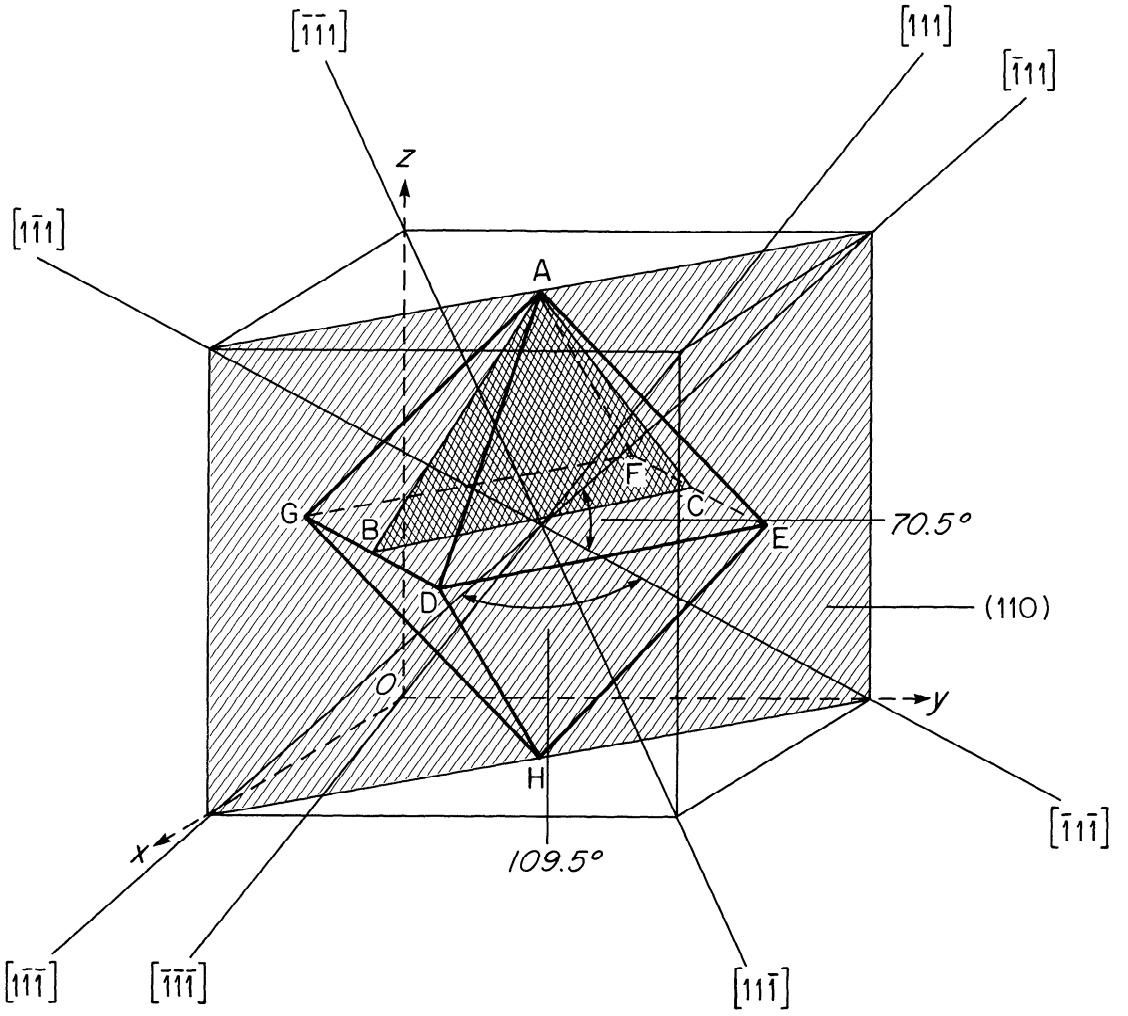

Figure 2. Sketch of a magnetite octahedron, showing the (110) plane (hatched) and eight <111> directions of easy magnetization.

5 K in a field of 2.5 T and then warmed to 300 K in approximately zero field. The observed sharp decrease in SIRM at a Verwey transition temperature T_V = 122 K indicates almost stoichiometric magnetite [*Özdemir et al.*, 1993].

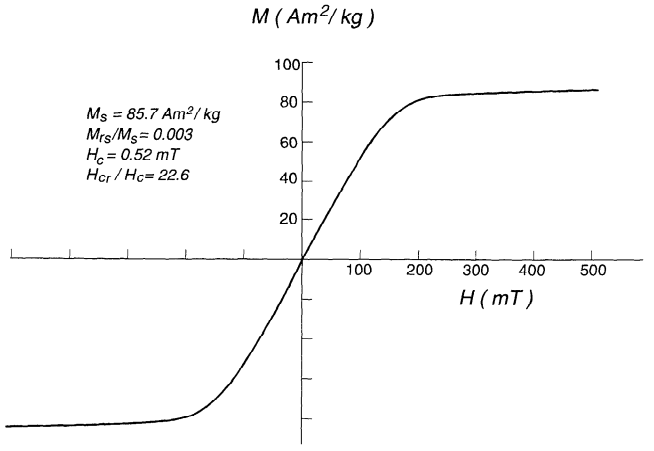

Figure 3. Room temperature hysteresis loop for the 3-mm octahedral magnetite crystal. The hysteresis parameters indicate true multidomain behavior.

Domain Observations on a {110} Crystal Plane

Patterns Away From Crystal Boundaries

On a strain-free {110} surface away from the edge of the polished section, we observe large domains with simple shapes and straight boundaries (Figure 5a). $\mathbf{M_S}$ in each domain lies along one of four <111> directions in the plane of view (Figures

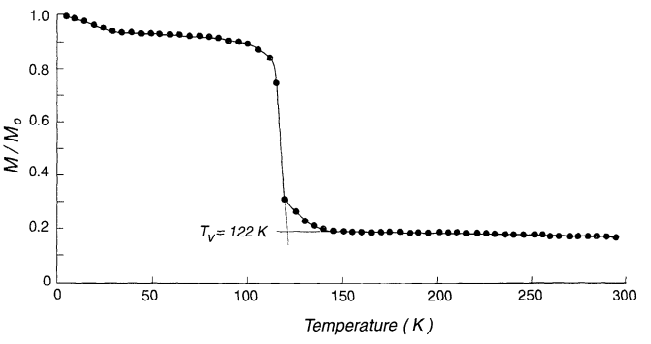

Figure 4. Normalized saturation isothermal remanence (SIRM) curve of the single crystal of magnetite during warming from 5 K to 300 K in zero field. A sharp Verwey transition at T_V = 122 K indicates stoichiometric Fe_3O_4.

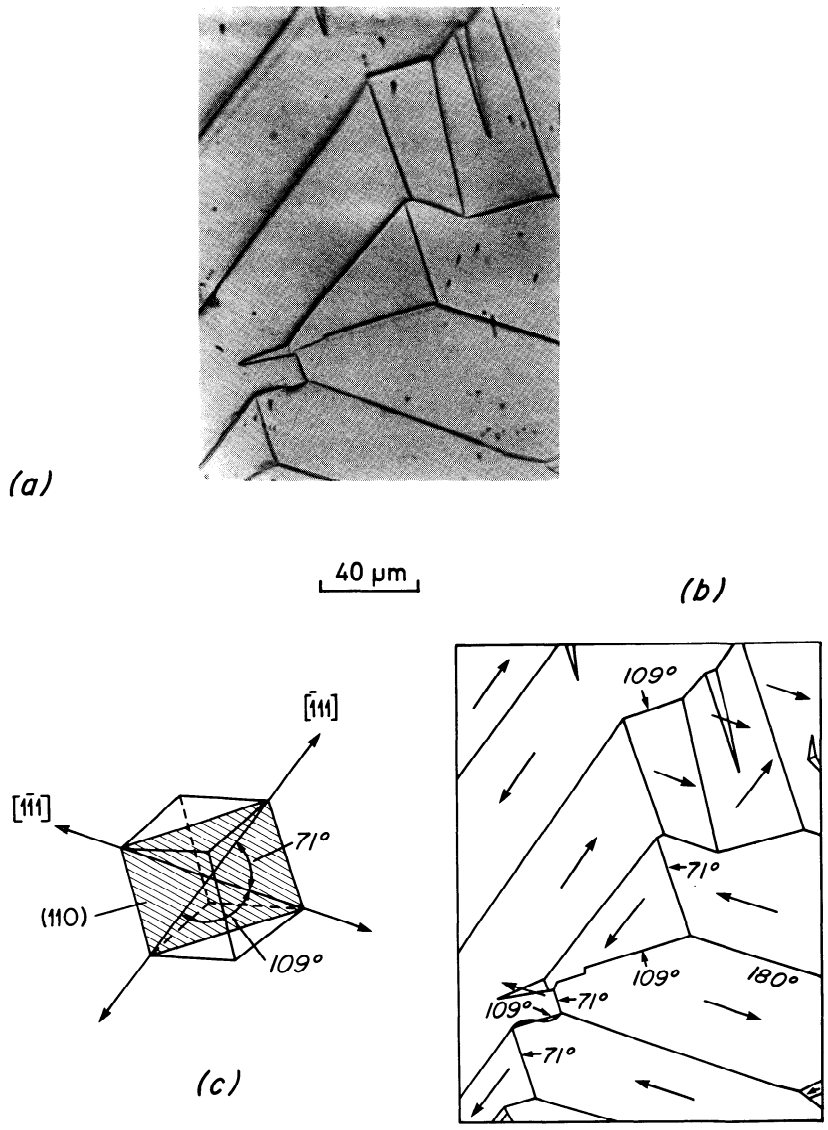

Figure 5. (a) Domain patterns observed on a {110} surface away from a crystal edge. (b) Inferred domain magnetization directions. All $\mathbf{M}_S$ vectors are parallel to the viewing surface. (c) {110} surface which contains [1$\bar{1}$1] and [$\bar{1}$11] easy axes. Magnetostatic and magnetocrystalline energies are minimized, and no magnetic poles or demagnetizing structures appear on the viewing surface.

5b and 5c). The various body domains are separated by 71°, 109°, or 180° walls, all with about equal visibility. Because $\mathbf{M}_S$ is able to follow magnetocrystalline easy directions without producing poles at the viewing surface, sectioning the crystal parallel to {110} has little effect on the domain structure that would exist inside the unsectioned crystal. The main change is a reduction in the dimensions of the original crystal, which should affect the number and spacing of domains but not their shape or $\mathbf{M}_S$ orientation. Thus we believe the patterns in Figure 5 and subsequent {110} views are representative of internal domain structures.

Figure 6 is another example of simple body domains typical of the crystal interior, magnetized along [$\bar{1}$11] and [1$\bar{1}$1] axes and separated by 71°, 109°, and 180° walls. Apart from minor curvature and offsets, the walls are basically straight and parallel.

A feature of much interest is the formation of several closure domains at the margin of the chemically altered region at the top right. In this region, magnetite has been oxidized and completely replaced by hematite. Although this is not a crystal boundary, it is a magnetic boundary because hematite is only weakly ferromagnetic. Thus domain configurations can be strongly influenced by chemical alteration of a crystal.

Patterns Near Internal Boundaries

Figure 7 illustrates a system of body and surface closure domains resembling that proposed in Figure 1b. The 180° body domains are magnetized parallel to the [$\bar{1}$11] and [1$\bar{1}\bar{1}$] easy directions. Closure domains form where the body domains meet a deep crack at the top of the diagram. The magnetization in the closure domains is parallel to the easy [1$\bar{1}$1] and [$\bar{1}$1$\bar{1}$] directions. Each closure domain is bounded by one 71° and one 109° wall. The flux circuit is closed within the crystal by the closure domains.

A series of en echelon spikes, magnetized reversely to the body domains they penetrate, flank either side of the zigzag

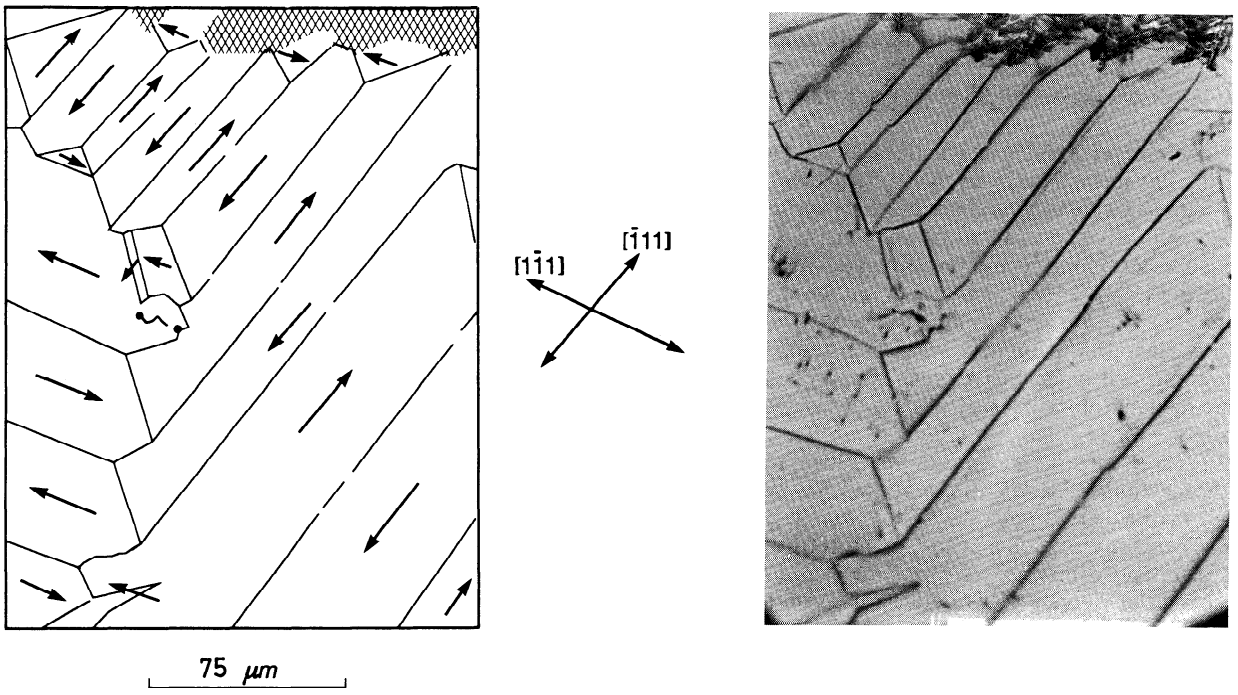

Figure 6. Interior domain patterns observed on a {110} surface away from crystal boundaries. The body domains are magnetized along [$\bar{1}$11] and [1$\bar{1}$1] easy axes and separated by 71°, 109°, and 180° walls. Notice the closure domains at the margin of the chemically altered region at the top.

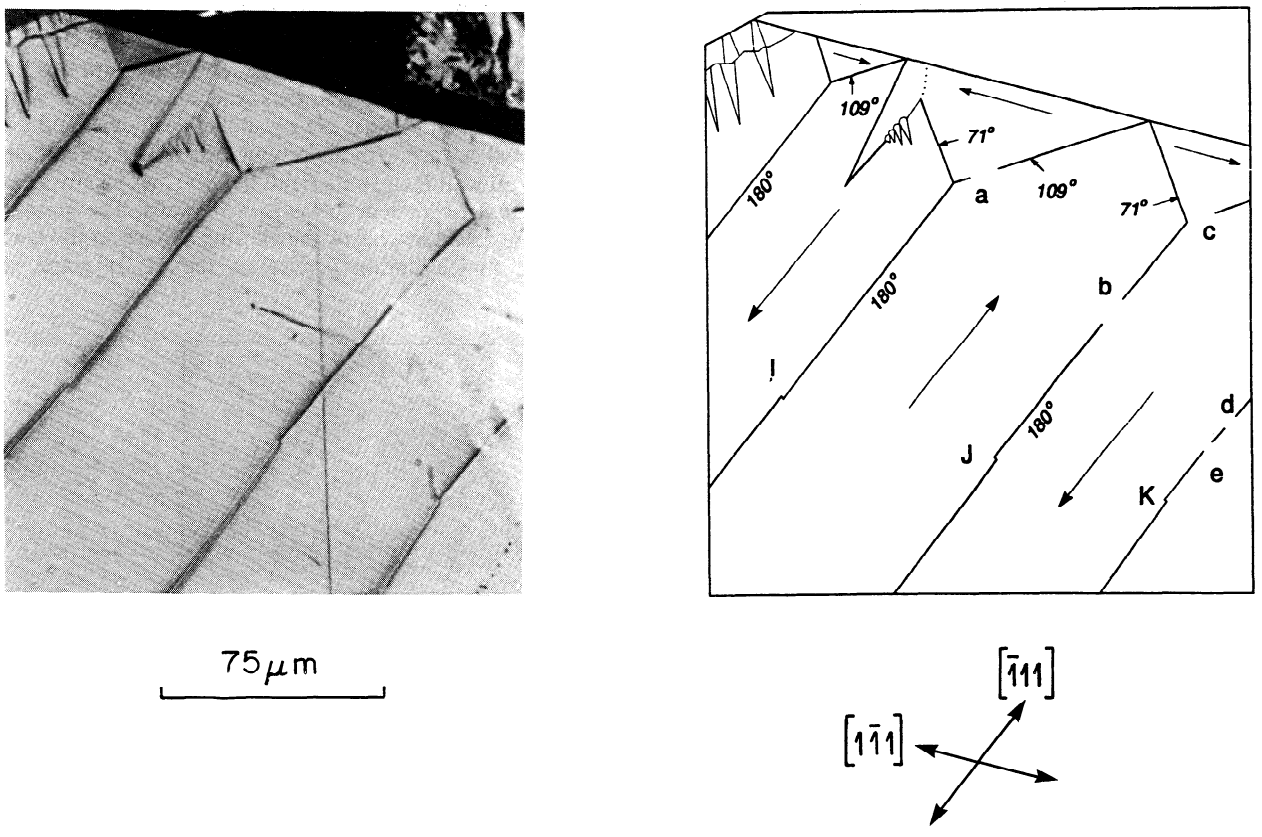

Figure 7. Closure domain patterns observed on a {110} surface along a deep crack and inferred domain magnetization directions along [1$\bar{1}$1] and [$\bar{1}$11]. The closure domains along the crack have perfect 71° and 109° walls. Notice the linear feature (labeled abd) and the kinks (labelled IJK). A reverse spike domain occurs between two closure domains.

109°(?) wall in the upper left corner of the diagram. We infer that alternate segments of the zigzag carry poles of opposite signs. Each segment forms the base of a spike, which serves to offset the demagnetizing field of poles on that segment [*Néel*, 1944].

A large reverse spike magnetized along the [$\bar{1}11$] easy direction has formed between the 71° and 109° walls at the upper left. One side bears a series of minor subsidiary demagnetizing spikes. The main structure, consisting of a pair of closure domains plus a central reverse spike, was first proposed by *Lifshitz* [1944]. Reverse spikes are the main means of reducing surface poles in uniaxial materials, where closure domains cannot form, but they are also common in magnetite, for example when the flux circuit cannot be completed by closure domains alone because of uneven spacing of the body domains.

In Figure 7, several sections of the domain walls have not attracted colloid particles. Less colloid has settled on the section marked a and no colloid is on section c of the 109° walls. There are also "colloid gaps" in the 180° walls (b, d, e). Gaps a, b, and d line up. We propose that a linear defect underlying the viewing plane deflects the wall spins, so that they locally rotate parallel to the plane of view and attract less colloid.

An interesting feature in Figure 7 is the series of "kinks" (I, J, K) in the 180° domain walls. These kinks line up almost parallel to the [$1\bar{1}1$] easy direction. The kinks probably mark Bloch lines, at which the direction of interior rotation of spins in the Bloch wall reverses. Similar observations were made by *DeBlois and Graham* [1958] and *Shtrikman and Treves* [1960a], who postulated that the sign of poles on the edge of the wall switches along the length of the wall. In the first segment the Bloch transition is a right-handed screw, giving north polarity on the edge, whereas in the second segment the Bloch transition is a left-handed screw, yielding south polarity on the edge of the wall.

Figure 8 gives another example of an array of body and closure domains formed along a crystal crack. The kinks (I and J) in the 180° Bloch walls probably mark the locations of Bloch lines. In the body domains, $\mathbf{M_s}$ is along <111> easy directions, but because the crack changes direction, this is probably not the case for all the closure domains. The upper part of the crack has the same favorable orientation as in Figures 1b and 7, so that $\mathbf{M_s}$ in the two upper closure domains can follow a <111> easy direction while also being parallel to both the viewing surface and the plane of the crack. In the lower two closure domains, $\mathbf{M_s}$ is likely rotated away from <111> to be more nearly parallel to the crack, as sketched.

An interesting domain structure forms at the corner point P where the two cracks meet and merge. The resulting magnetic poles around this surface imperfection create a large demagnetizing field, which is offset by a reversely magnetized closure domain on the left of the crack. Flux closes in a loop that crosses the grain boundary and involves two interacting closure domains of opposite magnetization. Surface irregularities of this kind are known to act as nucleating centers for domains of reverse magnetization [*Goodenough*, 1954; *Shtrikman and Treves*, 1960b]. Judging by our observations, nucleation could occur on either side of the boundary.

Patterns Near a Crystal Edge

Closure domain structures formed near a crystal edge differ considerably from closure domains along cracks and other internal grain boundaries. The domain patterns in Figure 9 were observed along the edge (AB in Figure 2) where the (110) viewing plane (triangle ABC) intersects the ($1\bar{1}1$) crystal surface (triangle ADG). The body domains are magnetized along [$1\bar{1}1$], at right angles to the crystal edge, as expected. However, the walls bounding the closure domains are not at the anticipated angles of 125° and 145° to the 180° walls, and some of them make angles distinctly <90° with each other.

Another curious feature in Figure 9 is that the closure domain walls collect colloid particles unevenly. The right-hand wall of each closure domain images much heavier than the left-hand wall. This observation suggests uncompensated poles on the right-hand walls.

There are also major colloid gaps between the closure domains and the body domains, so much so that these two appear almost as separate systems. The gaps form two lines, abcd and efgh, cutting across demagnetizing spikes as well as 180° walls. The two lines are parallel to each other and to the ($1\bar{1}1$) crystal surface. An underlying pair of line defects could have this effect if their stress fields deflect spins locally so as to weaken the field gradient above the 180° walls. The stress field from a line defect just below the viewing surface would tend to align the magnetization parallel to the {110} plane, thus

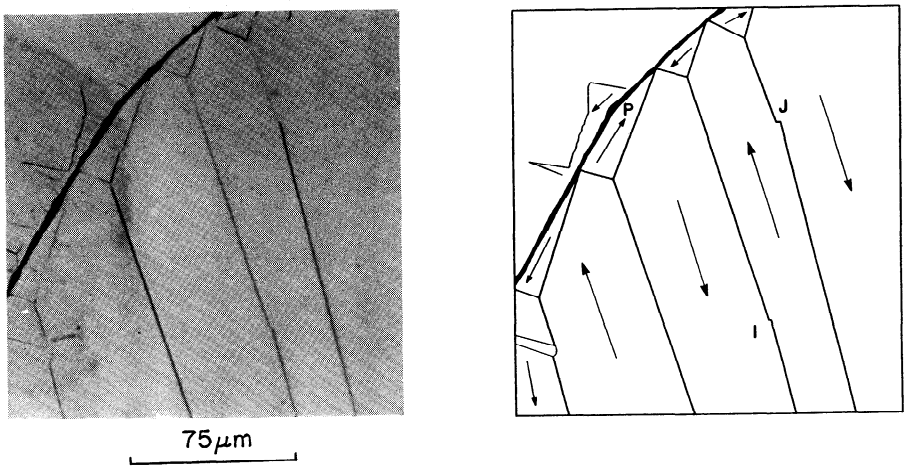

Figure 8. Closure domain patterns observed on a {110} surface along a crystal crack and inferred domain magnetization directions. At point P where the two cracks meet, a reverse closure domain forms on the other side of the crack in order to reduce the energy associated with surface poles around this crystal imperfection. The kinks (marked as I and J) probably indicate a change in the spin rotation in the wall.

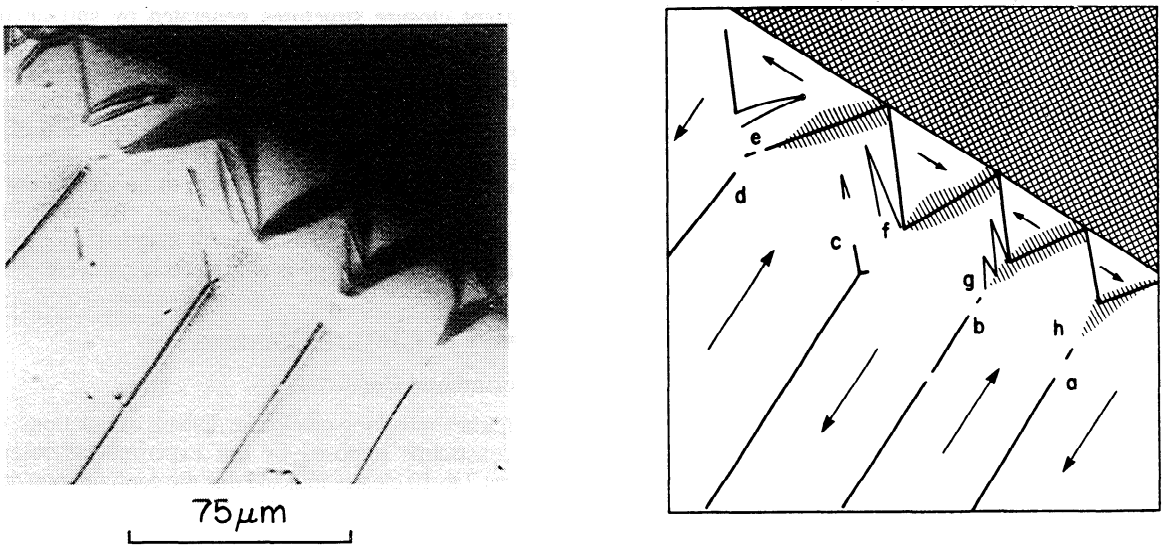

Figure 9. Closure domain patterns formed at the edge of the single crystal where the (110) viewing plane intersects the $(1\bar{1}1)$ crystal surface. The body domains are magnetized along $[1\bar{1}1]$ at right angles to the crystal edge. Magnetization directions in the closure domains are interpreted in the discussion section. Notice the uneven colloid distribution on the right-hand walls of the closure domains. Notice also the linear features labelled abcd and efgh which produce gaps in the body domain walls.

eliminating the stray field which attracts colloid. If so, it is a curious coincidence that the lines cross the crystal just at the terminations of the body domains.

Figure 10 shows another example of closure domains formed where 180° body domains intersect the $(1\bar{1}1)$ crystal edge. Instead of the expected unequal angles of 125° and 145°, the walls bounding closure domains make approximately equal angles with the 180° walls, like 90° walls. However, the angle between closure domain walls is consistently less than 90°. The symmetry of the closure domains suggests that $\mathbf{M_S}$ is rotated away from a <111> axis to be almost surface parallel, as sketched. However, the apparent symmetry is contradicted by the dense deposit of colloid along the left side of each closure domain. We will discuss later what this asymmetry tells us about magnetization directions in the closure domains.

Other interesting features in Figure 10 are the kinks and double kinks or possibly bows in the left-hand 180° wall and a small reverse spike domain anchored to a nonmagnetic inclusion. The inclusion generates poles, whose demagnetizing field is diminished by the spike.

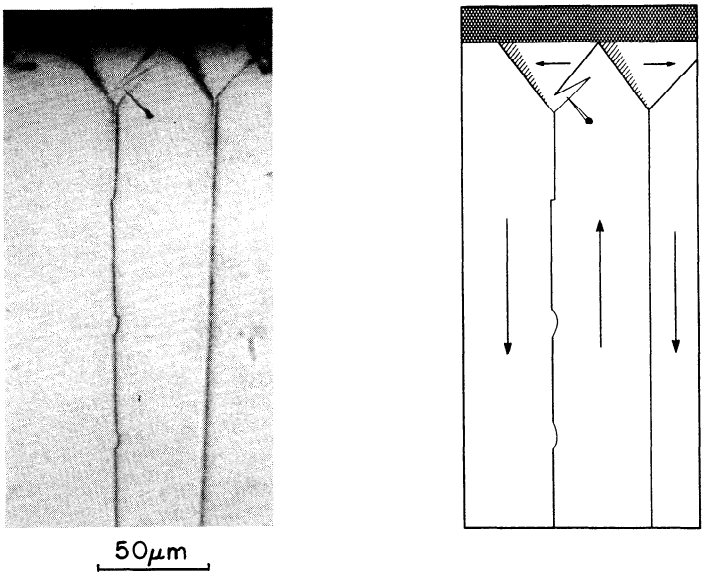

Figure 10. Closure domain patterns along the $(1\bar{1}1)$ crystal edge in a {110} viewing plane. The body domains intersect the crystal edge at right angles. The angle between closure domain walls is systematically less than 90°. Notice the dense deposit of colloid along the left-hand wall of each closure domain. A nonmagnetic inclusion in the body domain causes free magnetic poles which generate a small spike domain.

Domain Observations on a {111} Crystal Plane

The domain patterns in Figure 11a were observed on a {111} plane, corresponding to an octahedral crystal face (e.g., the (111) face ADE in Figure 2). The main features are three sets of parallel straight walls at 120° angles, with surface traces along $[11\bar{2}]$, $[\bar{1}21]$, and $[\bar{2}11]$. These principal walls are heavily decorated with colloid.

Four <111> easy axes cut the (111) face: [111] at 90° and $[11\bar{1}]$, $[1\bar{1}1]$, and $[\bar{1}11]$ at 19.5° (Figure 2). The latter axes project on the (111) plane as $[11\bar{2}]$, $[\bar{1}21]$, and $[\bar{2}11]$. We infer that the three sets of heavily decorated boundaries are the surface intersections of three sets of walls, separating domains in which $\mathbf{M_s}$ vectors are approximately parallel to $[11\bar{1}]$, $[1\bar{1}1]$, and $[\bar{1}11]$, respectively.

The surface pole density $\sigma = \mathbf{M_s}\cdot\hat{\mathbf{n}}$ will be reduced if $\mathbf{M_s}$ is deflected away from these axes toward the (111) plane. However, there must be some residual angle between $\mathbf{M_s}$ vectors and (111) because between the major walls there are prominent zigzag and coat hanger domain patterns which represent closure structures generated by surface poles on (111). In the model shown in Figure 11b, the arms of the coat hanger structures penetrate oppositely magnetized domains, reducing the net pole density and the magnetostatic energy. In some locations in Figure 11a, only the upper arm of the coat hanger is present, with a chain of reverse spikes suspended from it. The zigzag patterns seem to be a different style of structure, but their strategy is similar. By subdividing and interleaving domains with different magnetization directions, the magnetostatic energy is considerably reduced.

Theory of Closure Domains

Experimental Constraints

Before embarking on closure domain calculations, consider the constraints imposed by our experimental observations. Figures 7 to 10 clearly indicate that the configuration of closure domains viewed in a {110} plane depends strongly on the orientation of the crystal boundary at which the closure domains

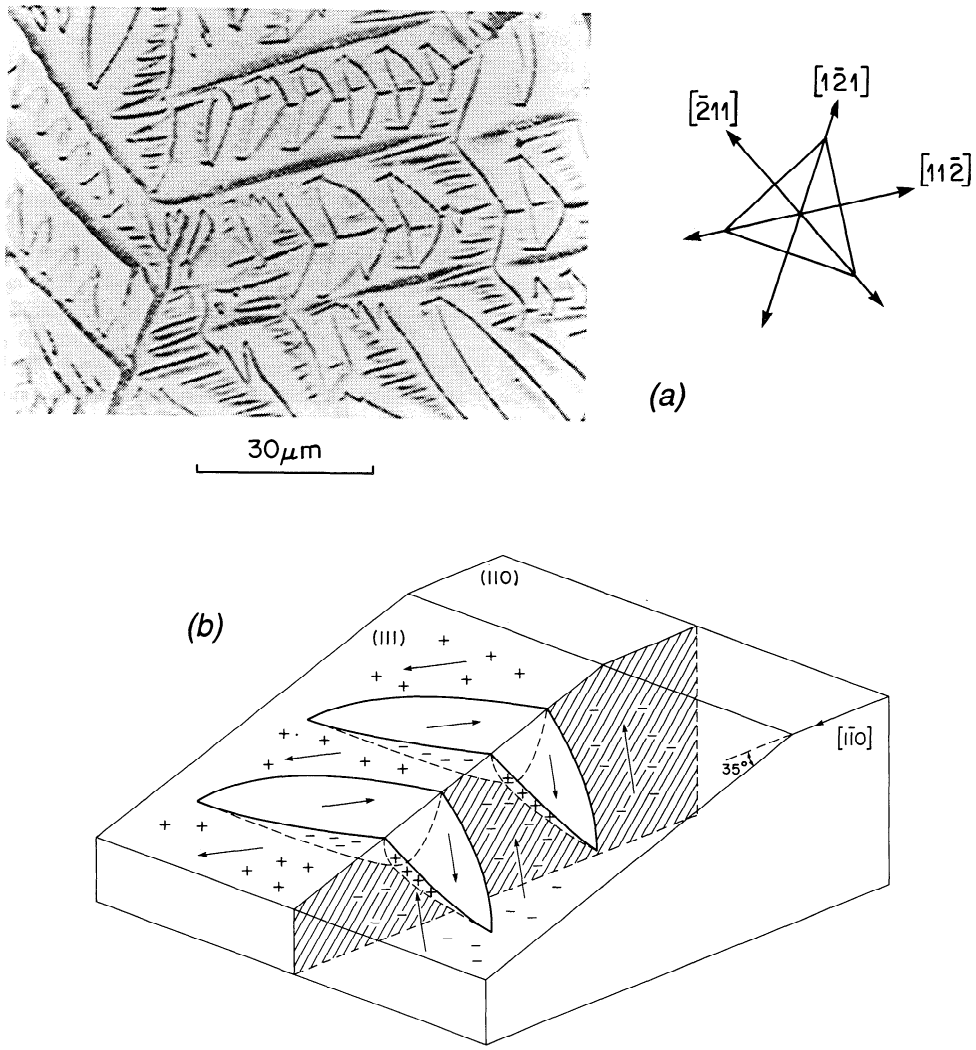

Figure 11. (a) Domain patterns on a {111} surface (the (111) face ADE in Figure 2) of the octahedral single crystal. The principal walls (thick lines) follow <112> directions, which are projections of <111> axes on the {111} surface. The intervening zigzag and coat hanger patterns are boundaries of partial surface closure domains. (b) A sketch of coat hanger patterns on a {111} crystal plane. When the viewing surface deviates from {110}, $\mathbf{M_s}$ vectors cut the surface and produce poles. The coat hanger domains act as partial closure domains, reducing the magnetostatic energy of the surface poles.

form. Cracks like those in Figures 7 and 8 which intersect the viewing plane along <111> are ideal boundaries for the formation of 71° and 109° walls because $\mathbf{M_S}$ in the closure domains can be simultaneously in an easy direction, minimizing magnetocrystalline anisotropy energy E_a, and parallel to the plane of the crack, eliminating surface poles and associated magnetostatic energy E_m. This situation was sketched in Figure 1b.

When closure domains form at a {111} crystal edge, as can be observed in Figures 9 and 10, E_m and E_a cannot be simultaneously minimized but are in competition in deciding the direction of $\mathbf{M_S}$. If $\mathbf{M_S}$ lies along a <111> easy axis (Figure 1c), so that 71° and 109° walls form (125° and 145° angles between closure and body domain walls), E_a is minimized, but poles appearing on the {111} surface increase E_m. If $\mathbf{M_S}$ is surface parallel (Figure 1a), so that closure domains are bounded by 90° walls (making 135° angles with the 180° walls), poles on {111} are eliminated but E_a increases.

The real situation at a {111} crystal edge may be intermediate. Near the boundary where pole demagnetizing fields are strongest, $\mathbf{M_S}$ may be nearly surface parallel, while away from the boundary, $\mathbf{M_S}$ may rotate gradually toward the nearest easy axis (the μ^* effect [*Lifschitz*, 1944; *Néel*, 1944; *Shockley*, 1948]). When $\mathbf{M_S}$ rotates within a domain, there is a new source of E_m: volume poles with a density $\rho = \nabla \cdot \mathbf{M_S}$.

Experimentally (Figures 9 and 10), closure domains at {111} boundaries are almost symmetrical in form, resembling Figure 1a rather than Figure 1c. These observations imply that E_m (tending to produce a surface-parallel $\mathbf{M_S}$) outweighs E_a. The symmetry is actually not perfect. The two "90°" walls make angles significantly <90° with each other, and they gather colloid unevenly. We will interpret these effects later.

For the present calculations, we adopt the following simplified picture. Closure domain walls are separated by 90° angles. The shapes of the closure domains change with the angle θ between $\mathbf{M_S}$ and the {111} surface so as to eliminate surface poles on the closure domain walls, the shapes shown for θ= 0 (Figure 1a) and θ= 19.5° (Figure 1c) being the extremes.

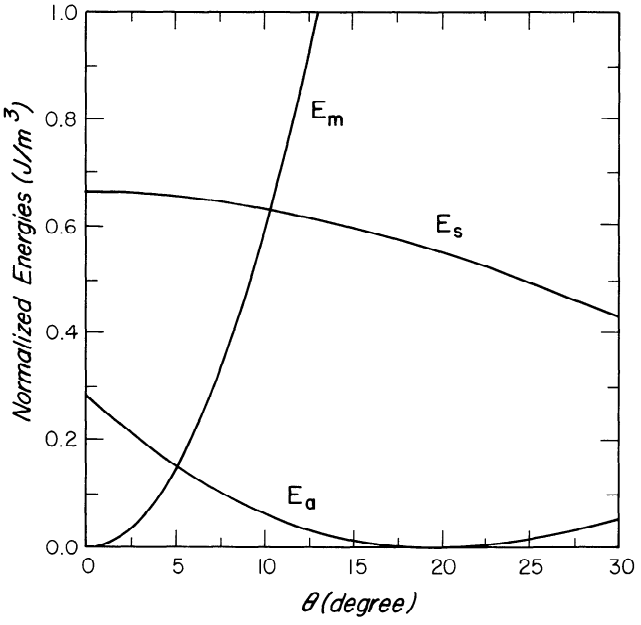

Figure 12. Variation of the magnetostatic energy E_m, magnetocrystalline anisotropy energy E_a, and magnetostriction energy E_s with the angle θ between $\mathbf{M_{sc}}$ and the crystal edge (compare Figures 13 and A1).

We ignore volume poles and changes in the direction of $\mathbf{M_S}$ within closure domains. The full calculation is given in the appendix. The results are summarized in Figure 12.

Calculation of the Direction of $\mathbf{M_S}$ in Closure Domains

As anticipated, E_a is minimum when θ= 19.5° ($\mathbf{M_S}$ along <111>) and E_m is minimum when θ= 0 ($\mathbf{M_S}$ along <112>, parallel to the {111} crystal surface). Magnetoelastic energy E_s, arising from the incompatible magnetostrictions of the body and closure domains, decreases continuously as θ increases, i.e., as the $\mathbf{M_S}$ vector in the closure domain rotates toward $\mathbf{M_S}$ in the body domains. The equilibrium value θ_{eq} of 2.2°, obtained by setting $d(E_a+E_m+E_s)/d\theta = 0$, is determined mainly by the sharp increase in E_m as $\mathbf{M_S}$ deflects away from the {111} surface (Figure 12). Our estimate is very close to the θ_{eq}= 1.8° obtained by *Stacey* [1963] using a different approach.

Thus pole avoidance is the main concern in determining closure domain configurations. This theoretical result explains our experimental observation (Figures 9 and 10) that closure domains at a {111} crystal edge in magnetite are bounded by approximately 90° walls, as in iron, and not by 71° and 109° walls.

Calculation of Equilibrium Domain Size

Although E_m is the most influential energy term in determining the direction of $\mathbf{M_S}$ in the closure domains, E_s makes a much larger contribution to the total energy at θ_{eq} (Figure 12). The balance between E_s and the wall energy E_w then determines the equilibrium width L of the body and closure domains. In a large crystal, E_w is contributed mainly by the body domain walls. For a simple lamellar array of 180° walls, each with area A and wall energy γ per unit area, extending across the width d of the crystal,

$$E_w = \gamma A d/L. \tag{1}$$

Assuming that the same array of closure domains exists at both top and bottom surfaces of the crystal, we have from the appendix

$$E_s \approx 9\lambda_{111}^2 c_{44} AL/4 \tag{2}$$

Setting the derivative of E_w+E_s with respect to L equal to zero, we find the equilibrium domain width L_{eq} as a function of grain size d:

$$L_{eq} = (4\gamma d/9\lambda_{111}^2 c_{44})^{1/2} \tag{3}$$

Equation (3) predicts that closure and body domains like those we observe in large grains are stable in much smaller grains also, and provides the scaling law to predict their sizes and numbers as a function of grain size d.

Discussion

Our observations of closure domains formed at free surfaces, such as crystal edges and internal grain boundaries and cracks, confirm the early theoretical prediction [*Landau and Lifschitz*, 1935] that the formation of closure domains greatly reduces magnetostatic energy and is therefore energetically favored in crystals like magnetite. Our experimental results suggest strongly that stray fields due to pole formation will be avoided as far as possible, on the surface as well as within the body of a magnetite crystal, and that closure domains are the favored mechanism for eliminating poles.

Further evidence that the magnetostatic energy plays a primary role in controlling domain structures in magnetite is the fact that closure domains change their shape depending on the crystallographic orientation of the boundary at which they form. When the boundary intersects a {110} viewing plane along a <111> easy axis, the closure domains are asymmetric in shape and are bounded by 71° and 109° walls (Figures 7 and 8) like those in the interior away from boundaries (Figures 5 and 6). But when the boundary is a {111} crystal face, containing no <111> easy axis, the closure domains are symmetric and bounded by ≈90° walls (Figures 9 and 10), suggesting that $\mathbf{M_S}$ has been deflected away from <111> almost into parallelism with the surface in order to reduce pole formation. Our calculations confirm that E_m is much more effective than E_a in rotating $\mathbf{M_S}$.

The Structure of Closure Domains

Type 1. Type 1 closure domains, which form when the bounding surface intersects the viewing plane along or nearly along <111> (Figures 7 and 8), have the following characteristics:

1. The closure domain is asymmetric in shape.
2. Each closure domain is bounded by one 71° and one 109° wall.
3. Closure and body domains are magnetized in <111> easy directions.

This favorable orientation promotes flux closure within the crystal and minimizes both E_m and E_a. The domain spacing is determined by the balance between wall energy in the body of the crystal and excess magnetoelastic energy in the closure domains (equation (3); see also *Özdemir and Dunlop* [1993]).

Type 2. Type 2 closure domains formed at a {111} crystal edge appear to be different in general (Figures 9, 10, and 13). Their features are as follows:

1. The closure domain is almost symmetric in shape.
2. Each closure domain is bounded by what appear to be ≈90° walls.
3. The magnetization in the 180° body domains is along a <111> easy axis, perpendicular to the crystal edge.
4. The magnetization in the closure domain is predicted to be almost, although not exactly, surface parallel. The fine structures observed on a {111} viewing plane (Figure 11) show that $\mathbf{M_S}$ does intersect this surface, generating some poles, but the angle of intersection is calculated to be only ≈2°.
5. The angle α between the two closure domain walls is systematically less than 90° and varies as a function of 180° domain spacing L. In Figures 9 and 10, α varies in the range 72°-84° and 78°-80°, respectively.
6. The closure domain walls formed at a crystal edge collect colloid particles unevenly, indicating the presence of magnetic poles along one of the two closure domain boundaries.

Figure 13 compares three models for the internal structure of type 2 closure domains. In Figure 13a, $\mathbf{M_S}$ is almost surface parallel and has been rotated ≈20° away from a <111> easy axis. E_a is much increased compared to the body domains, and the closure domains require an internal magnetic field to maintain their magnetization in this unfavorable direction. This field is supplied by the demagnetizing field of surface poles appearing on {111}. Figure 13b shows the extreme case in which $\mathbf{M_S}$ lies along a <111> axis, producing a large pole density and consequent demagnetizing field.

The pole fields are strongest near the surface, and so it is logical that $\mathbf{M_S}$ should be deflected by a large angle at the surface but should rotate toward <111> as one moves away from the surface (the μ* effect: Figure 13c). This model reduces magnetostatic energy overall, but the poles released at the crystal edge spread into the crystal as volume poles.

An inhomogeneous $\mathbf{M_S}$ within closure domains complicates calculations considerably. Qualitatively, however, it is easy to see that it will lead to a blanket of colloid over the closure domain, since the volume poles will be more or less uniformly distributed, and a concentration of colloid where the surface poles are densest on closure domain walls, namely, away from the {111} surface. In Figures 9 and 10, however, the colloid concentration seems to increase toward the {111} surface.

The model of Figure 13b can explain both observed features 5 and 6. In the limiting case sketched in Figure 14, the closure domain is bounded by a 71° and a 109° wall. The angle between the walls is 70°, which is around the lower limit of the distribution of α observed. $\mathbf{M_{sc}}$ and $\mathbf{M_{s2}}$ make equal angles of 35° with the 109° wall, so that $\sigma_{net}=0$ on this wall. However, $\mathbf{M_{s1}}$ and $\mathbf{M_{sc}}$ make unequal angles of 35° and 75°, respectively, with the 71° wall. This wall therefore carries poles with density $\sigma = M_s \sin 35° - M_s \sin 75°$ and gathers colloid. With this geometry, every left-hand 71° closure domain wall will be similarly decorated. If $\mathbf{M_{sc}}$ is downward and to the right, instead of upward and to the right as shown, the decorated 71° walls will be on the right.

The structure of Figure 13b can explain the observations, but it is not obvious why this structure should occur. The structures of Figures 13a and A1, which minimize poles on the surface and eliminate them on closure domain walls, have much lower energies.

Crystal Defects, Zones of Alteration, and Grain Boundaries

Our observations show that crystal defects such as inclusions, cracks, grain boundaries and chemically altered regions in the crystal affect the domain structure of magnetite. Examples are given in Figures 6-10.

In Figure 10, a small nonmagnetic inclusion acts as a "hole" in the uniformly magnetized domain, with the result that poles appear on the boundary of the inclusion. The magnetostatic energy would be quite large without the reversely magnetized spike domain anchored to the inclusion. Its effect is to redistibute the poles and reduce their density. Similarly, the sets of spikes attached to closure domain walls in Figure 7 offset poles appearing on these boundaries.

Sharp bends and corners, for example, where grain boundaries or cracks change direction (point P in Figure 8), are defects which can serve as nucleation sites for reverse domains. The large demagnetizing field developed at a corner can be offset by creating an oppositely magnetized domain on the other side of the boundary, as we observe.

"Colloid gaps" are common features of 180° walls, e.g., in Figures 7 and 9. Our interpretation is that linear defects (dislocations) underlying the viewing plane locally deflect spins in the walls they cross, reducing the field gradient above the wall. "Kinks" in walls (Figures 7, 8, and 10) probably have a similar cause: reversal of spin rotation in the wall at Bloch lines [*Shtrikman and Treves*, 1960a]. However, the kinks can move along the walls because the Bloch lines are not anchored to defects.

A novel and interesting observation is that chemical alteration affects domain structure, as shown in Figure 6. A hematized region of the crystal acts as a magnetic boundary and is flanked by closure domains. As alteration spreads through the crystal, the closure domains will form intricate networks, profoundly changing both the body domain structure and the remanence of the crystal. To our knowledge, this is the first observation of a direct link between magnetic mineral alteration and domain structure changes responsible for remagnetization.

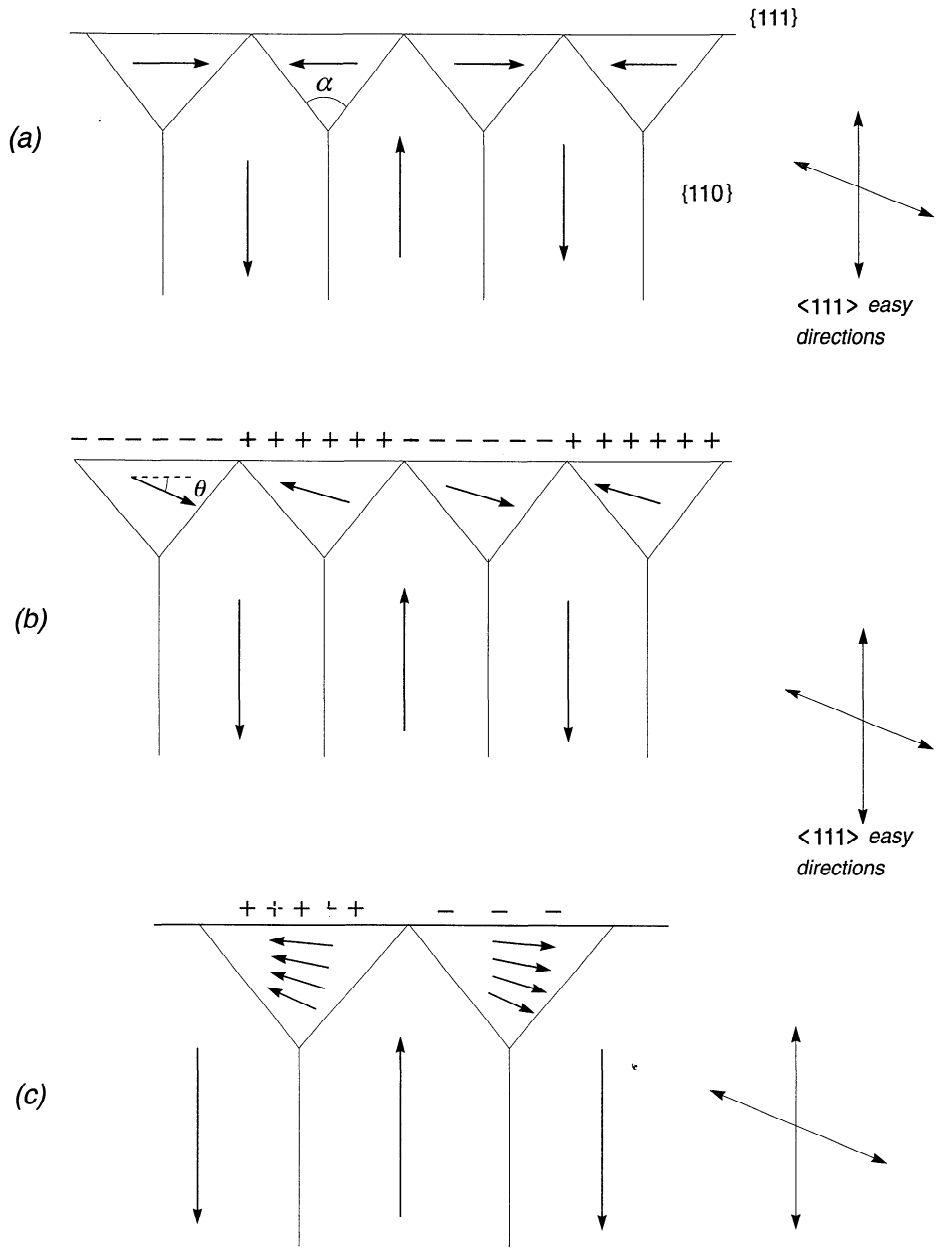

Figure 13. Model closure domain structures formed at the edge where the (110) viewing plane intersects the $(1\bar{1}1)$ crystal surface. (a) If closure domains are not magnetized in an easy direction, they have excess magnetocrystalline energy and require an internal magnetic field to maintain their magnetization in this unfavorable orientation. (b) When the magnetization in the closure domain makes an angle θ with the crystal edge, the resulting surface poles will produce a strong demagnetizing field. (c) At the crystal edge, the closure domain magnetization rotates away from the easy direction to be nearly edge parallel under the influence of the demagnetizing field. Surface poles are thereby reduced, but volume poles appear within the closure domains.

Why Are Closure Domains Seldom Observed in Magnetite?

While we have experienced no problems in observing closure domains either along internal boundaries such as cracks and alteration zones or at crystal edges, other authors have seldom observed them. Although one would not expect large arrays of regular closure domains in small magnetite grains (<10 μm, say), it is curious that they have not been observed in ≈100-μm grains. We believe this is due principally to the lack of orientation of the viewing plane in most previous studies. Although body domain walls may show through in unfavorably oriented sections, such as {111}, extraneous fine structures due to surface poles obscure any closure structures that might be present. Only on an accurately oriented {110} surface is it straightforward to view arrays of lamellar 180° domains terminating in closure domains.

The lack of observations of closure domains in magnetite has sometimes been attributed to the existence of a macrostress that induces a strong uniaxial anisotropy, making the formation of closure domains energetically unfavorable [*Worm et al.*, 1991; *Ye and Merrill*, **1995**]. We estimate the macrostress required to eliminate closure domains in magnetite by comparing the magnetostatic energy E_m for a lamellar array of 180° domains with the magnetoelastic energy $E_s = (3/2)\lambda_s \sigma V_c$ of

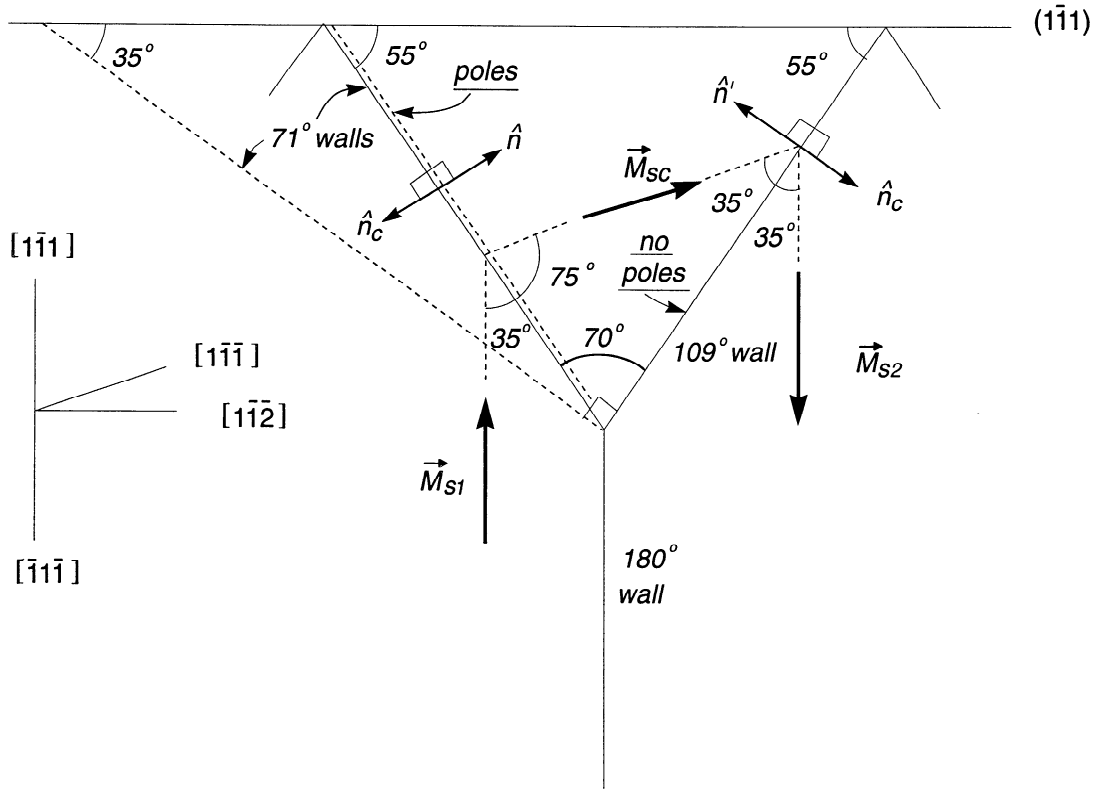

Figure 14. A possible model for heavy colloid concentration on one side of closure domains at a crystal edge. The 71° and 109° walls make an angle <90° with each other, as observed experimentally. As a result, the left-hand wall makes unequal angles of 35° and 75° with $\mathbf{M_{s1}}$ and $\mathbf{M_{sc}}$, respectively, and poles appear on this wall.

closure domains (see the appendix for symbols and equations; the saturation magnetostriction $\lambda_s = 40\times10^{-6}$ for magnetite). The body domains are magnetized along the uniaxial easy axis induced by the stress σ. By allowing wavy walls at the crystal surface (resembling the zigzag structures we observe in Figure 11a), E_m can be reduced to about one-half the value given by (A1) [*Rosenberg and Tănăsoiu*, 1969].

Setting $E_m = E_s$, we obtain σ ≈ 650 MPa or 6.5 kbar. Since the breaking stress for magnetite is ≈250 MPa [*Soffel*, 1966], we conclude that closure domains in magnetite are not suppressed by stress.

"Missing Domains Paradox"

The fact that fewer body domains are generally observed on titanomagnetite grains of a given size (especially for $Fe_{2.4}Ti_{0.6}O_4$ or TM60) than are predicted theoretically [e.g., *Worm et al.*, 1991] has been cited as evidence that these grains frequently, or even typically, occupy metastable local energy minimum (LEM) states [*Moon and Merrill*, 1984], containing fewer than the equilibrium number of domains. There is ample evidence that metastable LEM states exist. Metastable single-domain states are particularly important [e.g., *Halgedahl and Fuller*, 1983; *Boyd et al.*, 1984; *Halgedahl*, 1991]. However, some recent work claims that metastable LEM states are the only significant remanence mechanism in multidomain magnetite [e.g., *Shcherbakov et al.*, 1993], to the exclusion of domain wall displacements [e.g., *Néel*, 1955; *Dunlop and Xu*, 1994; *Xu and Dunlop*, 1994].

In any paradox, suspicion falls first on the theory. The one-dimensional micromagnetic predictions of *Moon and Merrill* [1985] have been widely cited [e.g., *Van der Voo*, 1993]. By its very nature, a one-dimensional model prohibits the formation of closure domains. By including surface closure structures of a prescribed form, *Ye and Merrill* [1991] showed that the expected number of domains is considerably less than that predicted by Moon and Merrill. *Xu et al.* [1994] carried through an unconstrained two-dimensional calculation for 1-μm and 5-μm magnetite grains and achieved further reductions in the predicted numbers of body domains. For 1-μm grains the predicted number agrees with *Smith*'s [1980] observations, while for 5-μm grains the "paradox" becomes marginal.

The key feature of Xu et al.'s calculations is that closure domains, which were not present in the starting model, appeared spontaneously in the course of successive energy minimizations. *Williams and Dunlop* [1990] predicted similar structures in unconstrained three-dimensional calculations for <1-μm magnetite grains. These calculations are the first clear demonstration that closure domains are not an artifact of highly constrained calculations like those of *Landau and Lifschitz* [1935], *Kittel* [1949], or *Worm et al.* [1991] but emerge in a natural way from unconstrained theories.

Although for technical reasons, closure domains have been poorly resolved in many previous studies, our observations leave no doubt that they are a typical feature of the interior domain structure in magnetite. As a result, we seriously question the "missing domains paradox." When closure domains are taken into account, theory predicts very nearly the number of body domains that are actually observed in magnetite (although the situation may be different in TM60). It follows that domain-wall displacements in grains containing a fixed, near-equilibrium number of body domains [e.g., *Néel*, 1955] remain a viable mechanism of remanence in magnetite.

Conclusions

1. We observe arrays of closure domains terminating 180° body domains in a single crystal of magnetite viewed on a {110} polished surface. Our observations confirm the prediction of *Landau and Lifschitz* [1935] that closure domains should be the favored means of reducing magnetostatic energy in strongly magnetic materials like magnetite. Previous studies probably failed to resolve arrays of closure domains because the viewing surfaces were unoriented and did not contain two sets of <111> easy axes.

2. Closure domains formed along favorably oriented boundaries, such as cracks, in the interior of the crystal are asymmetrical and are bounded by 71° and 109° walls. The magnetization in each closure domain lies in an easy direction and is also parallel to the boundary, thus minimizing both magnetocrystalline and magnetostatic energies.

3. Closure domains formed along the crystal edge where the {110} viewing plane intersects the {111} crystal surfaces are symmetrical and are bounded by what appear to be ≈90° walls, but the angle between the walls is less than the expected 90°. Furthermore, one of each pair of closure domain walls gathers much more colloid than the other, indicating a concentration of poles. According to our interpretation, the magnetization in the body domains is almost at right angles to the surface, while the magnetization in the closure domains is rotated away from an easy direction so as to be more nearly parallel to the surface, thus reducing surface poles and magnetostatic energy. Several models are proposed to explain the concentration of colloid on one set of closure domain walls, but none is entirely convincing.

4. Domain structures in magnetite are very sensitive to crystal defects, such as voids, inclusions, dislocations, grain boundaries (especially sharp bends), and chemically altered regions. All of these can generate closure domains and/or reverse spikes and thus can serve as nucleating sites for reverse domains.

5. Our theoretical calculations predict that (1) the magnetization in closure domains at a crystal edge is within ≈2° of being parallel to the free surface; (2) closure domains greatly reduce the predicted numbers of body domains in magnetite and reconcile domain observations with theory; (3) closure domains occur in much smaller magnetites than those we have examined, their widths scaling with grain sized as $\sqrt{d}$ (equation (3)); and (4) stress is not a viable mechanism for suppressing closure domains in magnetite.

Appendix: Magnetic Energies of Closure Domains

The magnetic energies considered below are for closure domains viewed in the (110) plane (ABC in Figure 2), intersecting the $(1\bar{1}1)$ crystal surface (ADG) along the $[1\bar{1}\bar{2}]$ axis (AB). For the body domains, $\mathbf{M_s}$ lies in the (110) plane, parallel to $[1\bar{1}1]$, i.e., perpendicular to the $(1\bar{1}1)$ surface. For the closure domains, $\mathbf{M_s}$ lies in (110) at a variable angle θ to $[1\bar{1}\bar{2}]$ (Figure A1).

The closure domains change shape depending on θ because of the requirement that surface poles be eliminated on internal boundaries, i.e., that $\sigma_{net} = \sum \mathbf{M_s}\cdot\hat{\mathbf{n}} = 0$ in crossing domain boundaries. The geometry then requires that the $\mathbf{M_s}$ vectors in the body and closure domains make equal angles $(90° \pm \theta)/2$ with the closure domain walls (see Figure A1). When $\theta = 0$ ($\mathbf{M_s}$ parallel to the $(1\bar{1}1)$ surface), the closure domains have the shape of a right-angled isosceles triangle bounded by 90° walls (Figure 1a), and when $\theta = 19.5°$ ($\mathbf{M_s}$ parallel to $[1\bar{1}\bar{1}]$), the closure domains are asymmetric right-angled triangles with interior angles of 35° and 55°, bounded by 71° and 109° walls (Figure 1c).

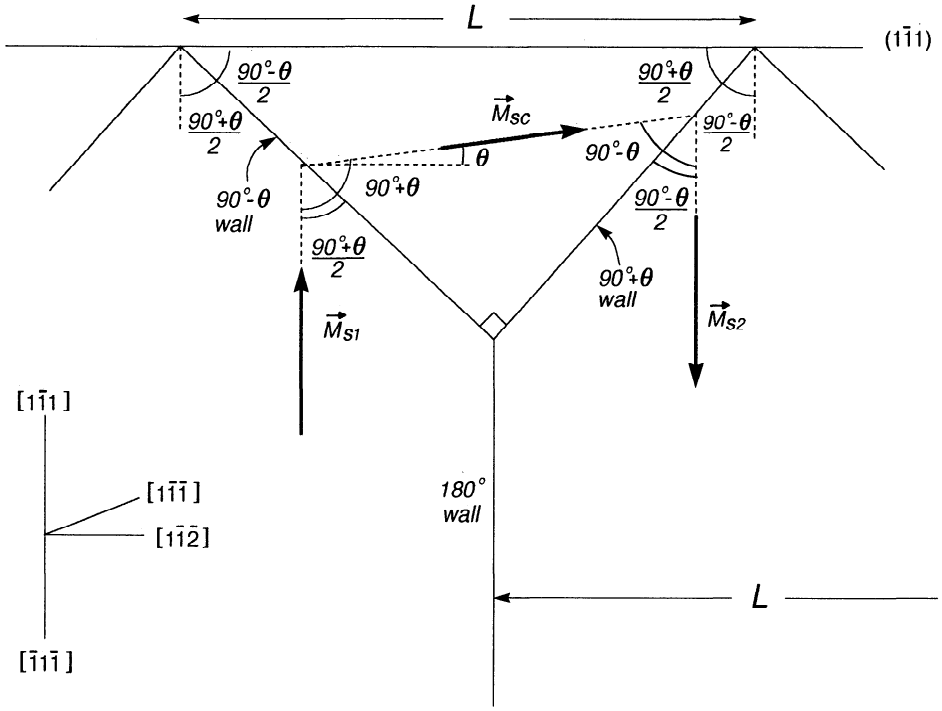

Figure A1. The closure domain geometry used in the appendix for calculating the magnetization direction $\mathbf{M_{sc}}$ in closure domains and the equilibrium domain spacing L as a function of grain size.

Magnetostatic Energy E_m

E_m is associated with poles appearing on the $(1\bar{1}1)$ surface with density $\sigma = \mathbf{M_s}\cdot\hat{\mathbf{n}} = M_s \sin\theta$. It is given by [e.g., *Kittel*, 1949]

$$E_m = 8.53\times10^{-8} \sin^2\theta\, M_s^2 AL. \quad \text{(A1)}$$

This expression assumes a single set of lamellar 180° body domains, each of width L, crossing the entire grain (of width $d>>L$) and terminating at both $(1\bar{1}1)$ and $(\bar{1}1\bar{1})$ surfaces (each of area A) in closure domains. For magnetite, $M_s = 480$ kA/m at room temperature.

Magnetocrystalline Anisotropy Energy E_a

We consider only the excess E_a when M_s deviates from the $[1\bar{1}1]$ easy axis. E_a can be written generally as [e.g., *Kittel*, 1949; *Chikazumi*, 1964]

$$E_a = K_1 V_c (\alpha_1^2\alpha_2^2 + \alpha_2^2\alpha_3^2 + \alpha_3^2\alpha_1^2 - 1/3), \quad \text{(A2)}$$

where the α_i are the direction cosines of $\mathbf{M_s}$ with respect to the <100> axes, V_c is the total volume of the closure domains (top and bottom surfaces), and the magnetocrystalline anisotropy constant $K_1 = -1.36\times10^4$ J/m^3 for magnetite at room temperature [*Syono*, 1969]. Higher-order terms have been neglected. The α_i are related to θ by

$$\alpha_1 = \alpha_2 = \sin\theta/\sqrt{3} + \cos\theta/\sqrt{6},$$
$$\alpha_3 = \sin\theta/\sqrt{3} - 2\cos\theta/\sqrt{6}. \quad \text{(A3)}$$

From Figure A1, after some trigonometry, the volume of each closure domain is $L^2\cos\theta/4$. There are $2d/L$ closure domains (top and bottom surfaces), giving

$$V_c = \tfrac{1}{2}d^2L\cos\theta = \tfrac{1}{2}AL\cos\theta. \quad \text{(A4)}$$

Magnetoelastic Energy E_s

E_s originates from the incompatible magnetostrictions of the closure and body domains. Assuming that the resulting elastic deformation is accommodated fully by the closure domains, we can write

$$E_s = E_{s0} - (3/2)\lambda_{100}V_c(\sigma_{11}\alpha_1^2 + \sigma_{22}\alpha_2^2 + \sigma_{33}\alpha_3^2)$$
$$- 3\lambda_{111}V_c(\sigma_{12}\alpha_1\alpha_2 + \sigma_{23}\alpha_2\alpha_3 + \sigma_{31}\alpha_3\alpha_1), \quad \text{(A5)}$$

where E_{s0} is the magnetoelastic energy when there are no closure domains. In (A5), the α_i refer to $\mathbf{M_s}$ in the closure domains, while the stress tensor σ_{ij} results from the magnetostriction of the body domains. With the body domains magnetized along $[1\bar{1}1]$, we have [*Kittel*, 1949; *Brown*, 1963] $\sigma_{11} = \sigma_{22} = \sigma_{33}$ and $\sigma_{12} = \sigma_{23} = \sigma_{31} = c_{44}\lambda_{111}$, where the elastic constant $c_{44} = 9.55\times10^{10}$ N/m^2 [*Doraiswami*, 1947] and the magnetostriction constant $\lambda_{111} = 78.2\times10^{-6}$ [*Moskowitz*, 1993] for magnetite at room temperature. Dropping the λ_{100} term in (A5), which contributes only a constant since $\alpha_1^2+\alpha_2^2+\alpha_3^2=1$, and rewriting, we have

$$E_s = 3\lambda^2_{111}c_{44}V_c(1 - \alpha_1\alpha_2 - \alpha_2\alpha_3 - \alpha_3\alpha_1), \quad \text{(A6)}$$

where α_i and V_c as a function of θ are specified by (A3) and (A4), respectively.

Acknowledgments. We thank Gordon Nord for his illuminating suggestions about magnetization directions in Figure 5 and Viktor Hoffmann for his help and advice on polishing and observing techniques. Bob Ramik and Malcolm Back donated the single crystal of magnetite. Wyn Williams and an anonymous referee provided helpful reviews. Khader Khan, Alison Dias, and Carolyn Moon were of great assistance in producing the figures and text. This work was sponsored by the Natural Sciences and Engineering Research Council of Canada through research grant A7709 to D.J.D.

References

Bogdanov, A.A., and A.Y. Vlasov, Domain structure in a single crystal of magnetite, *Izv. Earth Phys.*, *1*, 49-58, 1965.

Boyd, J.R., M. Fuller, and S.L. Halgedahl, Domain wall nucleation as a controlling factor in the behaviour of fine magnetic particles in rocks, *Geophys. Res. Lett.*, *11*, 193-196, 1984.

Brown, W.F., Jr., *Micromagnetics*, 144 pp., John Wiley, New York, 1963.

Chikazumi, S., *Physics of Magnetism*, 554 pp., John Wiley, New York, 1964.

DeBlois, R.W., and C.D. Graham Jr., Domain observations on iron whiskers, *J. Appl. Phys.*, *29*, 931-939, 1958.

Doraiswami, M.S., Elastic constants of magnetite, pyrite and chromite, *Proc. Indian Acad. Sci.*, *25*, 413-416, 1947.

Dunlop, D.J., and S. Xu, Theory of partial thermoremanent magnetization in multidomain grains, 1, Repeated identical barriers to wall motion (single microcoercivity), *J. Geophys. Res.*, *99*, 9005-9023, 1994.

Elscher, B., and W. Andrä, Magnetische Elementorbezirke, *Fortschr. Phys.*, *3*, 163-171, 1955.

Goodenough, J.B., A theory of domain creation and coercive force in polycrystalline ferromagnetics, *Phys. Rev.*, *95*, 917-932, 1954.

Halgedahl, S.L., Magnetic domain patterns observed on synthetic Ti-rich titanomagnetite as a function of temperature and in states of thermoremanent magnetization, *J. Geophys. Res.*, *96*, 3943-3972, 1991.

Halgedahl, S.L., and M. Fuller, The dependence of magnetic domain structure upon magnetization state with emphasis upon nucleation as a mechanism for pseudo-single domain behavior, *J. Geophys. Res.*, *88*, 6505-6522, 1983.

Heider, F., S.L. Halgedahl, and D.J. Dunlop, Temperature dependence of magnetic domains in magnetite crystals, *Geophys. Res. Lett.*, *15*, 499-502, 1988.

Hoffmann, V., R. Schäfer, E. Appel, A. Hubert, and H. Soffel, First domain observations with the magneto-optical Kerr effect on Ti-ferrites in rocks and their synthetic equivalents, *J. Magn. Magn. Mater.*, *71*, 90-94, 1987.

Kittel, C., Physical theory of ferromagnetic domains, *Rev. Mod. Phys.*, *21*, 541-583, 1949.

Landau, L., and E. Lifshitz, On the theory of the dispersion of magnetic permeability in ferromagnetic bodies, *Phys. Z.*, *8*, 153-169, 1935.

Lifshitz, E., On the magnetic structure of iron, *J. Phys. USSR.*, *8*, 337-346, 1944.

Moon, T., and R.T. Merrill, The magnetic moments of non-uniformly magnetized grains, *Phys. Earth Planet Inter.*, *34*, 186-194, 1984.

Moon, T., and R.T. Merrill, Nucleation theory and domain states in multidomain magnetic material, *Phys. Earth Planet Inter.*, *37*, 214-222, 1985.

Moskowitz, B.M., High-temperature magnetostriction of magnetite and titanomagnetites, *J. Geophys. Res.*, *98*, 359-371, 1993.

Néel, L., Quelques propriétés des parois de domains élémentaires ferromagnétiques, *Cah. de Phys.*, *25*, 1-20, 1944.

Néel, L., Some theoretical aspects of rock magnetism, *Adv. Phys.*, *4*, 191-242, 1955.

Özdemir, Ö., and D.J. Dunlop, Magnetic domain structures on a natural single crystal of magnetite, *Geophys. Res. Lett.*, *20*, 1835-1838, 1993.

Özdemir, Ö., and D. York, ^{40}Ar/^{39}Ar laser dating of biotite inclusions in a single crystal of magnetite, *Geophys. Res. Lett.*, *19*, 1799-1802, 1992.

Özdemir, Ö., D.J. Dunlop, and B.M. Moskowitz, The effect of oxidation on the Verwey transition in magnetite, *Geophys. Res. Lett.*, *20*, 1671-1674, 1993.

Rosenberg, M., and C. Tănăsoiu, Magnetic domains, in *Magnetic Oxides*, part 2, edited by D.J. Craik, pp. 483-573, John Wiley, New York, 1975.

Shcherbakov, V.P., E. McClelland, and V.V. Shcherbakova, A model of multidomain thermoremanent magnetization incorporating temperature-variable domain structure, *J. Geophys. Res.*, *98*, 6201-6216, 1993.

Shockley, W., Energy calculations for domains, *Phys. Rev.*, *73*, 1246, 1948.

Shtrikman, S., and D. Treves, Internal structure of Bloch walls, *J. Appl Phys.*, *31*, 147S-148S, 1960a.

Shtrikman, S., and D. Treves, On the resolution of Brown's paradox, *J. Appl. Phys.*, *31*, 725-735, 1960b.

Soffel, H.C., Stress dependence of the domain structure of natural magnetite, *Z. Geophys.*, *32*, 345-361, 1966.

Soffel, H.C., C. Aumüller, V. Hoffmann, and E. Appel, Three-dimensional domain observations of magnetite and titanomagnetites using the dried colloid SEM method, *Phys. Earth Planet. Inter.*, *65*, 43-53, 1990.

Smith, P.P.K., The application of Lorentz electron microscopy to the study of rock magnetism, *Inst. Phys. Conf. Ser.*, *52*, 125-128, 1980.

Syono, S., Magnetocrystalline anisotropy and magnetostriction of Fe_3O_4 - Fe_2TiO_4 series, with special application to rock magnetism, *Jpn. J. Geophys.*, *4*, 71-143, 1965.

Stacey, F.D., The physical theory of rock magnetism, *Adv. Phys.*, *12*, 45-133, 1963.

Van der Voo, R., *Paleomagnetism of the Atlantic, Tethys and Iapetus Oceans*, 411 pp., Cambridge University Press, New York, 1993.

Williams, W., and D.J. Dunlop, Some effects of grain shape and varying external magnetic fields on the magnetic structure of small grains of magnetite, *Phys. Earth Planet. Inter.*, *65*, 1-14, 1990.

Williams, W., R.J. Enkin, and G. Milne, Magnetic domain wall visibility in Bitter pattern imaging, *J. Geophys. Res.*, *97*, 17,433-17,438, 1992.

Worm, H-U., P.J. Ryan, and S.K. Banerjee, Domain size, closure domains, and the importance of magnetostriction in magnetite, *Earth Planet. Sci. Lett.*, *102*, 71-78, 1991.

Xu, S., and D.J. Dunlop, Theory of partial thermoremanent magnetization in multidomain grains, 2, Effect of microcoercivity distribution and comparison with experiment, *J. Geophys. Res.*, *99*, 9025-9033, 1994.

Xu, S., D.J. Dunlop, and A.J. Newell, Micromagnetic modelling of two-dimensional domain structures in magnetite, *J. Geophys. Res.*, *99*, 9035-9044, 1994.

Ye, J., and R.T. Merrill, Differences between magnetic domain imaging observations and theory, *Geophys. Res. Lett.*, *18*, 593-596, 1991.

Ye, J., and R.T. Merrill, Residual stress and domain structure, *J. Geophys. Res.*, in press, 1995.

D. J. Dunlop and Ö. Özdemir, Department of Physics, Erindale College, University of Toronto, 3359 Mississauga Road North, Mississauga, Ontario, Canada L5L 1C6. (e-mail: ozdemir@physics.utoronto.ca)

S. Xu, NirvCentre, 401 Richmond St.W., Ste. 104, Toronto, Ontario, Canada M5V 3A8.

(Received May 20, 1994; revised October 26, 1994; accepted November 2, 1994.)